Article

Spectroscopic Studies of Metal Binding and Metal Selectivity in *Bacillus subtilis* BSco, a Homologue of the Yeast Mitochondrial Protein Sco1p

Luisa Andruzzi, Michiko Nakano, Mark J. Nilges, and Ninian J. Blackburn

J. Am. Chem. Soc., **2005**, 127 (47), 16548-16558• DOI: 10.1021/ja0529539 • Publication Date (Web): 02 November 2005

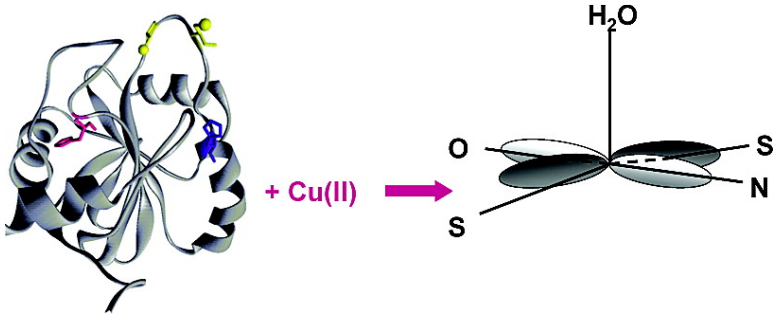

More About This Article

Additional resources and features associated with this article are available within the HTML version:

- Supporting Information
- Links to the 2 articles that cite this article, as of the time of this article download
- Access to high resolution figures
- Links to articles and content related to this article
- Copyright permission to reproduce figures and/or text from this article

View the Full Text HTML

J|A|C|S
ARTICLES
Published on Web 11/02/2005

Spectroscopic Studies of Metal Binding and Metal Selectivity in *Bacillus subtilis* BSco, a Homologue of the Yeast Mitochondrial Protein Sco1p

Luisa Andruzzi,[†] Michiko Nakano,[†] Mark J. Nilges,[‡] and Ninian J. Blackburn*,[†]

Contribution from the Department of Environmental and Biomolecular Systems, OGI School of Science and Engineering at OHSU, Beaverton, Oregon 97006-8921, and the Illinois EPR Research Center, University of Illinois at Urbana−Champaign, 600 South Mathews Avenue, Urbana, Illinois 61801

Received May 5, 2005; E-mail: ninian@ebs.ogi.edu

Abstract: Sco1 is a mitochondrial membrane protein involved in the assembly of the Cu_A site of cytochrome *c* oxidase. The *Bacillus subtilis* genome contains a homologue of yeast Sco1, YpmQ (hereafter termed BSco), deletion of which leads to a phenotype lacking in caa_3 (Cu_A-containing) oxidase activity but expressing normal levels of aa_3 (quinol) oxidase activity. Here, we report the characterization of the metal binding site of BSco in its Cu(I)-, Cu(II)-, Zn(II)-, and Ni(II)-bound forms. Apo BSco was found to bind Cu(II), Zn(II), and Ni(II) at a 1:1 protein/metal ratio. The Cu(I) protein could be prepared by either dithionite reduction of the Cu(II) derivative or by reconstitution of the apo protein with Cu(I). X-ray absorption (XAS) spectroscopy showed that Cu(I) was coordinated by two cysteines at 2.22 ± 0.01 Å and by a weakly bound low-*Z* scatterer at 1.95 ± 0.03 Å. The Cu(II) derivative was reddish-orange and exhibited a strong type-2 thiolate to Cu(II) transition around 350 nm. Multifrequency electron paramagnetic resonance (EPR), electron−nuclear double resonance (ENDOR), and electron spin-echo envelope modulation (ESEEM) studies on the Cu(II) derivative provided evidence of one strongly coupled histidine residue, at least one strongly coupled cysteine, and coupling to an exchangeable proton. XAS spectroscopy indicated two cysteine ligands at 2.21 Å and two O/N donor ligands at 1.95 Å, at least one of which is derived from a coordinated histidine. The Zn(II) and Ni(II) derivatives were 4-coordinate with $MS_2N(His)X$ coordination. These results provide evidence that a copper chaperone can engage in redox chemistry at the metal center and may suggest interesting redox-based mechanisms for metalation of the mixed-valence Cu_A center of cytochrome *c* oxidase.

Introduction

Cytochrome *c* oxidase is the terminal oxidase of the respiratory chain in mammals and in many bacteria.[1−4] It belongs to a family of integral membrane proteins that catalyze the four-electron reduction of molecular oxygen to water and couple the redox free energy released from the reaction to the formation of a proton motive force across the membrane that can be used for the synthesis of ATP.[5,6] This superfamily of oxidases can be divided into two categories.[3,4,7] The first branch can be exemplified by cytochrome *c* oxidase which makes use of cytochrome *c* as a reducing substrate and contains three redox centers, heme *a*, the heme a_3-Cu_B binuclear O_2-reducing site in subunit I, and the binuclear Cu_A electron-transfer site in subunit II.[7−19] A second branch can be exemplified by cyto-

* To whom correspondence should be addressed. Phone: (503)748-1384. Fax: (503)748-1464.
[†] OGI School of Science and Engineering at OHSU.
[‡] University of Illinois at Urbana−Champaign.

(1) Malmstrom, B. G. *Arch. Biochem. Biophys.* **1990**, *280*, 233−241.
(2) Babcock, G. T.; Wikstrom, M. *Nature* **1992**, *356*, 301−308.
(3) Garcia-Horsman, J. A.; Barquera, B.; Rumbley, J.; Ma, J.; Gennis, R. B. *J. Bacteriol.* **1994**, *176*, 5587−5600.
(4) Richter, O. M.; Ludwig, B. *Rev. Physiol. Biochem. Pharmacol.* **2003**, *147*, 47−74.
(5) Hosler, J. P.; Ferguson-Miller, S.; Calhoun, M. W.; Thomas, J. W.; Hill, J.; Lemieux, L.; Ma, J.; Georgiou, C.; Fetter, J.; Shapleigh, J.; Tecklenburg, M. M. J.; Babcock, G. T.; Gennis, R. B. *J. Bioenerg. Biomembr.* **1993**, *25*, 121−136.
(6) Calhoun, M. W.; Thomas, J. W.; Gennis, R. B. *Trends Biochem. Sci.* **1994**, *19*, 325−330.
(7) Blackburn, N. J.; de Vries, S.; Barr, M. E.; Houser, R. P.; Tolman, W. B.; Sanders, D.; Fee, J. A. *J. Am. Chem. Soc.* **1997**, *119*, 6135−6143.
(8) Iwata, S.; Ostermeier, C.; Ludwig, B.; Michel, H. *Nature* **1995**, *376*, 660−669.
(9) Tsukihara, T.; Aoyama, H.; Yamashita, E.; Tomizaki, T.; Yamaguchi, H.; Shinzawa-Itoh, K.; Nakashima, R.; Yaono, R.; Yoshikawa, S. *Science* **1995**, *269*, 1069−1074.
(10) Tsukihara, T.; Aoyama, H.; Yamashita, E.; Tomizaki, T.; Yamaguchi, H.; Shinzawa-Itoh, K.; Nakashima, R.; Yaona, R.; Yoshikawa, S. *Science* **1996**, *272*, 1136−1144.
(11) Ostermeir, C.; Harrenga, A.; Ermler, U.; Michel, H. *Proc. Natl. Acad. Sci. U.S.A.* **1997**, *94*, 10547−10533.
(12) Yoshikawa, S.; Shinzawa-Itoh, K.; Nakashima, R.; Yaono, R.; Yamashita, E.; Inoue, N.; Yao, M.; Fei, M. J.; Libeu, C. P.; Mizushima, T.; Yamaguchi, H.; Tomizaki, T.; Tsukihara, T. *Science* **1998**, *280*, 1723−1729.
(13) Soulimane, T.; Buse, G.; Bourenkov, G. P.; Bartunik, H. D.; Huber, R.; Than, M. E. *EMBO J.* **2000**, *19*, 1766−1776.
(14) Wilmanns, M.; Lapplalainen, P.; Kelly, M.; Sauer-Eriksson, E.; Saraste, M. *Proc. Natl. Acad. Sci. U.S.A.* **1995**, *92*, 11955−11959.
(15) Kroneck, P. M. H.; Antholine, W. A.; Riester, J.; Zumft, W. G. *FEBS Lett.* **1989**, *248*, 212−213.
(16) Kroneck, P. M.; Antholine, W. E.; Kastrau, D. H. W.; Buse, G.; Steffens, G. C. M.; Zumft, W. G. *FEBS Lett.* **1990**, *268*, 274−276.
(17) Farrar, J. A.; Neese, F.; Lappalainen, P.; Kroneck, P. M. H.; Saraste, M.; Zumft, W. G.; Thompson, A. J. *J. Am. Chem. Soc.* **1996**, *118*, 11501−11514.
(18) Slutter, C. E.; Sanders, D.; Wittung, P.; Malmstrom, B. G.; Aasa, R.; Richards, J. H.; Gray, H.; Fee, J. A. *Biochemistry* **1996**, *35*, 3387−3395.
(19) Williams, P. A.; Blackburn, N. J.; Sanders, D.; Bellamy, H.; Stura, E. A.; Fee, J. A.; McRee, D. E. *Nat. Struct. Biol.* **1999**, *6*, 509−516.

10.1021/ja0529539 CCC: $30.25

chrome bo_3 and aa_3-600 oxidases that use ubiquinol as a reducing substrate and lack the Cu_A site.[20−22]

Copper delivery to the Cu_A and Cu_B centers of the heme−copper oxidases is a complex process requiring a number of accessory proteins and chaperones.[23] Ctr1, a plasma-membrane transporter responsible for high-affinity copper uptake,[24−27] is proposed to deliver copper to Cox17,[28−31] which in turn delivers it to the mitochondrial membrane proteins Sco1 and Cox11[32] that have been implicated in the assembly of the Cu_A[33−36] and Cu_B[37−40] centers, respectively. However, the function of Sco is still under debate. Structural characterization of soluble domains of the *Bacillus subtilis* Sco1 homologue BSco by NMR[41] and X-ray diffraction (XRD),[42] and of human Sco1 by XRD,[43] showed that Sco1-type proteins exhibit a peroxiredoxin fold (Figure 1) similar to that of the well-known class of thioredoxin enzymes which catalyze thiol−disulfide redox switching. None of these structures contained bound copper at their CXXXC putative Cu(I) binding motif. Instead, the BSco crystal structure revealed both thiol and disulfide conformers, reinforcing the earlier proposal of Balatri et al., based on their NMR structure, that Sco could function in disulfide switching, possibly to reduce a disulfide formed between the two cysteine residues that bridge the Cox2 Cu_A binuclear center. A proteomic analysis of the localization of Sco homologues has extended the landscape of possible Sco functions even further.[44] Colocalization with genes encoding cyt *c*, multicopper oxidases, and Hyp1, a homologue of the periplasmic copper transporter CopC, has suggested that

1	MGQQIKDPLNYEVEPFTFQNQDGKNVSLES	30
31	LKGEVWLADFIFTNCETICPPMTAHMTDLQ	60
61	KKLKAENIDVRIISFSVDPENDKPKQLKKF	90
91	AANYPLSFDNWDFLTGYSQSEIEEFALKSF	120
121	KAIVKKPEGEDQVIHQSSFYLVGPDGKVLK	150
151	DYNGVENTPYDDIISDVKSASTLK	

Figure 1. Sequence data and NMR structure of BSco. The CETIC metal binding motif is shown in yellow, and the imidazole rings of the two possible histidine ligands are in red (H135) and purple (H55). The graphic was generated from PDB file 1ON4 by Weblab ViewerPro 3.5 (Accelerys).

Sco could exist as a multifunctional copper trafficking protein capable of interfacing among a number of different homeostatic pathways.

In a definitive study designed to investigate the functional role of copper, Winge and co-workers expressed a soluble truncated form of yeast Sco1p missing the N-terminal transmembrane helix, and they showed that it bound 1 mol of Cu(I) per monomer.[45] X-ray absorption spectroscopy on native and mutant forms of this construct provided good evidence that the Cu(I) is ligated via three ligands, C148 and C152 (within the conserved CXXXC motif) and the conserved H239. The mutation of any one of these residues resulted in diminished copper binding and a nonfunctional cytochrome *c* oxidase complex. Subsequent publication of the structures revealed that these residues were located on two solvent-exposed and conformationally mobile loops (in BSco numbering, the analogous residues are C45, C49, and H135). In the NMR structure, Cu(I) coordination by C45 and C49 could be well modeled, but the third ligand was less clear. Addition of Cu(II) to the protein was found to broaden the resonances of both the H135 and a second histidine (H55), suggesting that either or both residues could be involved in metal binding, but these histidines were located about 10−15 Å from the thiol S atoms in both the NMR and X-ray structures of apo BSco. Modeling of H135 along with C45 and C49 as copper ligands indicated that the conformational change required to bring H135 within coordinating distance did not violate structural constraints on the rest of the protein, and in the human Sco1 structure, all three putative Cu(I) binding ligands were in close proximity. However, definitive proof that H135 is the third copper ligand is still lacking.

In the present work, we explore further the structural properties of the metal binding site and report on the spectroscopic characterization of Cu(I)-, Cu(II)-, Zn(II)-, and Ni(II)-bound forms of the protein. XAS studies suggest that BSco employs a single metal site to bind all of these metals. Our results suggest a 2- or 3-coordinate site for Cu(I), similar to that previously reported for yeast Sco1p,[45] a 4- or 5-coordinate (tetragonal) site for Cu(II), and 4-coordinate sites for Zn(II) and Ni(II). ENDOR spectroscopy on the Cu(II) form has identified one strongly bound cysteine, a strongly coupled histidine, and

(20) Abramson, J.; Riistama, S.; Larsson, G.; Jasaitis, A.; Svensson-Ek, M.; Laakkonen, L.; Puustinen, A.; Iwata, S.; Wikstrom, M. *Nat. Struct. Biol.* **2000**, *7*, 910−917.
(21) Fann, Y. C.; Ahmed, I.; Blackburn, N. J.; Boswell, J. S.; Verkhovskaya, M. L.; Hoffman, B. M.; Wikstrom, M. *Biochemistry* **1995**, *34*, 10245−10255.
(22) van der Oost, J.; Lappalainen, P.; Musacchio, A.; Warne, A.; Lemieux, L.; Rumbley, J.; Gennis, R. B.; Aasa, R.; Pascher, T.; Malmstrom, B. G.; Saraste, M. *EMBO J.* **1992**, *11*, 3209−3217.
(23) Carr, H. S.; Winge, D. R. *Acc. Chem. Res.* **2003**, *36*, 309−316.
(24) Sharp, P. A. *Int. J. Biochem. Cell Biol.* **2003**, *35*, 288−291.
(25) Eisses, J. F.; Kaplan, J. H. *J. Biol. Chem.* **2002**, *277*, 29162−29171.
(26) Lee, J.; Pena, M. M.; Nose, Y.; Thiele, D. J. *J. Biol. Chem.* **2002**, *277*, 4380−4387.
(27) Puig, S.; Lee, J.; Lau, M.; Thiele, D. J. *J. Biol. Chem.* **2002**, *277*, 26021−26030.
(28) Glerum, D. M.; Shtanko, A.; Tzagoloff, A. *J. Biol. Chem.* **1996**, *271*, 14504−14509.
(29) Heaton, D. N.; George, G. N.; Garrison, G.; Winge, D. R. *Biochemistry* **2001**, *40*, 743−751.
(30) Srinivasan, C.; Posewitz, M. C.; George, G. N.; Winge, D. R. *Biochemistry* **1998**, *37*, 7572−7577.
(31) Abajian, C.; Yatsunyk, L. A.; Ramirez, B. E.; Rosenzweig, A. C. *J. Biol. Chem.* **2004**, *279*, 53584−53592.
(32) Horng, Y. C.; Cobine, P. A.; Maxfield, A. B.; Carr, H. S.; Winge, D. R. *J. Biol. Chem.* **2004**, *279*, 35334−35340.
(33) Mattatall, N. R.; Jazairi, J.; Hill, B. C. *J. Biol. Chem.* **2000**, *275*, 28802−28809.
(34) Bengtsson, J.; von Wachenfeldt, C.; Winstedt, L.; Nygaard, P.; Hederstedt, L. *Microbiology* **2004**, *150*, 415−425.
(35) Lode, A.; Kuschel, M.; Paret, C.; Rodel, G. *FEBS Lett.* **2000**, *485*, 19−24.
(36) Leary, S. C.; Kaufman, B. A.; Pellecchia, G.; Guercin, G. H.; Mattman, A.; Jaksch, M.; Shoubridge, E. A. *Hum. Mol. Genet.* **2004**, *13*, 1839−1848.
(37) Tzagoloff, A.; Capitanio, N.; Nobrega, M. P.; Gatti, D. *EMBO J.* **1990**, *9*, 2759−2764.
(38) Hiser, L.; Di Valentine, M.; Hamer, A. G.; Hosler, J. P. *J. Biol. Chem.* **2000**, *275*, 619−623.
(39) Carr, H. S.; George, G. N.; Winge, D. R. *J. Biol. Chem.* **2002**, *277*, 31237−31242.
(40) Banci, L.; Bertini, I.; Cantini, F.; Ciofi-Baffoni, S.; Gonnelli, L.; Mangani, S. *J. Biol. Chem.* **2004**, *279*, 34833−34839.
(41) Balatri, E.; Banci, L.; Bertini, I.; Cantini, F.; Ciofi-Baffoni, S. *Structure* **2003**, *11*, 1431−1443.
(42) Ye, Q.; Imriskova-Sosova, I.; Hill, B. C.; Jia, Z. *Biochemistry* **2005**, *44*, 2934−2942.
(43) Williams, J. C.; Sue, C.; Banting, G. S.; Yang, H.; Glerum, D. M.; Hendrickson, W. A.; Schon, E. A. *J. Biol. Chem.* **2005**, *280*, 15202−15211.
(44) Arnesano, F.; Banci, L.; Bertini, I.; Martinelli, M. *J. Proteome Res.* **2005**, *4*, 63−70.
(45) Nittis, T.; George, G. N.; Winge, D. R. *J. Biol. Chem.* **2001**, *276*, 42520−42526.

a more weakly coupled proton, probably derived from a solvent ligand. These results confirm the previous ligand assignments, and they provide evidence that this copper chaperone can engage in redox chemistry at the metal center, which may suggest interesting redox-based mechanisms for metalation of the mixed-valence Cu_A center of cytochrome *c* oxidase.

Experimental Section

Cloning and Expression of YpmQ. The clone for YpmQ was obtained from the *B. subtilis* library (accession number BG11622) and amplified using polymerase chain reactions (PCR) and oligonucleotides designed to introduce an NcoI restriction site at the 5′-end and a SapI restriction site at the 3′-end. The primers used were as follows: 5′-GTT TTT GTG TGC ATC CAT GGG ACA GCA GAT TAA AGA T-3′ (YpmQ forward primer) and 5′-GAA CTA AGC TCT TCC GCA CTT GAG TGT ACT GGC TGA-3′ (YpmQ reverse primer). PCR was performed using Deep Vent polymerase (Biolabs). The PCR product was digested with NcoI and SapI and cloned into the PTXB-3 expression vector (New England Biolabs). This allowed for a translational fusion of the MxeGyrA intein tag to the C-terminus of the target protein. The resulting plasmid was transformed into the *Escherichia coli* strain ER-2566. In a typical expression experiment, cultures were grown in a 1 L LB−glucose medium containing 100 μg/mL of ampicillin at 37 °C to a final A_{600} between 0.3 and 0.8. The cells were induced with 500 μM IPTG overnight in a shaker at 17 °C, harvested by centrifugation at 8500*g* for 30 min, and frozen at −80 °C. After thawing, the cells were resuspended in 50 mM phosphate buffer, 500 mM NaCl at pH 7.2 containing EDTA-free protease inhibitor (Roche), lysed in a French Press at 1000 psi, and centrifuged at 8500*g* for 30 min. The supernatant was filter sterilized through 0.45 μm syringe filters, and the volume was adjusted to 35 mL with column buffer and loaded onto a column of chitin beads. The protein was eluted off the column using sodium 2-mercaptoethanesulfonate, and eluted fractions were assayed by sodium dodecyl sulfate polyacrylamide gel electrophoresis (SDS-PAGE) on an Amersham Biosciences PHAST system (20% homogeneous gel). Fractions that contained BSco were pooled and concentrated in a Centriprep concentrator (molecular mass cutoff = 3 kDa) to about 10 mL. The concentrate was then ultrafiltered in a Centriprep (molecular mass cutoff = 10 kDa) and checked for purity by SDS-PAGE. No impurities were detected. The protein concentration was determined by Bradford analysis, and typical yields were 15−20 mg of pure BSco/L of culture. Electrospray mass spectrometry of the purified protein gave a mass of 19 759 Da. (The calculated mass for the sequence in Figure 1 including the N-terminal methionine with the CETIC (metal binding) motif present as a disulfide is 19 766 Da.)

Reconstitution with Cu(II), Zn(II), Ni(II), and Co(II). The reconstitution was performed in a Coy anaerobic chamber to prevent oxidation of the cysteine residues. Dithiothreitol (DTT) was added to the protein in a 10-fold excess relative to the protein concentration to reduce the cysteine residues in the CXXXC motif prior to metal reconstitution. Then, the protein was dialyzed overnight into 50 mM phosphate buffer at pH 7.2 to remove excess DTT, and 100 μL of an aqueous stock solution of the metal ion as a sulfate salt was added to obtain a 5-fold excess of M(II) in the final solution. Metal ion competition experiments were carried out in the same manner, except that 100 μL of a 1:1:1 aqueous solution of $CuSO_4$, $ZnSO_4$, and $NiSO_4$ was added in a 5-fold excess per metal salt. Excess metal ions were removed by exhaustive dialysis against the metal-free phosphate buffer. The bound metal was determined by inductively coupled plasma optical emission spectrometry (ICP-OES) on a Perkin-Elmer Optima 2000 DV spectrometer.

Reconstitution with Cu(I). The reconstitution was performed in an anaerobic chamber to prevent oxidation of the cysteine residues as described earlier.[46] DTT was added to the protein in a 10-fold excess to reduce the cysteine residues in the CXXXC motif prior to metal reconstitution. The excess DTT was removed by overnight dialysis into 50 mM phosphate buffer at pH 7.2 which also contained 10% acetonitrile. Copper was then added by slow infusion of a 100-fold stock solution of Cu(I) as the $[(CH_3CN)_4Cu^I]PF_6$ salt over a 1 h period, utilizing a syringe pump at a rate of 1 μL/min to a final ratio of 2:1 copper/protein. Successive dialyses were carried out against phosphate buffer containing 10%, 5%, and finally 0% acetonitrile. The bound copper concentration was determined by ICP-OES.

Spectroscopic Measurements. Electronic spectra were recorded on a Cary 50 scanning spectrophotometer. Quantitative EPR measurements were carried out on a Bruker ER085CS spectrometer at 77 K using a liquid nitrogen finger Dewar. Spectra were recorded at 20 mW power, 60 gain, and using a sweep time of 80 s. The concentration of paramagnetic copper was determined by double integration and referenced to a series of standard solutions of Cu(II) EDTA (50−200 μM $[Cu^{2+}]$ in 50 mM sodium phosphate buffer at pH 7.2) run in the same tube as the protein samples.

Multifrequency EPR, ENDOR, and ESEEM experiments were carried out at the University of Illinois, EPR Center. X-band EPR spectra were collected on a Varian E-122 spectrometer. The samples were run as frozen glasses at ∼80 K using liquid He and an Air Products Helitran cryostat. Q-band EPR spectra were collected on a Varian E-15 spectrometer with a Q-band TE011 cavity. Samples were run frozen at ∼105 K with a liquid N_2 flow cryostat. Pulsed ENDOR and ESEEM spectra were collected on a Bruker E580-10 Elexsys. Spectra were obtained at 20 K with a liquid He Oxford CF935 cryostat controlled by an Oxford ITC 4-temperature controller. Pulsed ENDOR experiments were obtained using a Davies three-pulse scheme ($\pi-T-\pi/2-\tau-\pi-\tau-$echo, with the RF pulse applied during time *T*). Two-dimensional three-pulse ESEEM experiments were obtained with a three-pulse scheme ($\pi/2-\tau-\pi/2-T-\pi/2-$echo) in which both τ and *T* are varied in time. Four-step phase cycling was used. The magnetic fields were calibrated with a Varian NMR Gauss meter. EPR and ENDOR spectra were simulated with the SIMPIPM program, developed at the University of Illinois, which is based on QPOW,[47] further details of which can be found in the Supporting Information.

X-ray absorption data were collected at the Stanford Synchrotron Radiation Laboratory. Cu (8.9 keV), Zn (9.6 keV), and Ni (8.3 keV) extended X-ray absorption fine structure (EXAFS) and X-ray absorption near edge structure (XANES) data were measured on beam line 9-3 using a Si[220] monochromator (crystal orientation $\varphi = 90°$) and an Rh-coated mirror upstream of the monochromator with a 13 keV energy cutoff to reject harmonics. Data were collected in fluorescence mode using a high-count-rate Canberra 30-element Ge array detector with maximum count rates below 120 kHz. A 6 μm Z-1 metal oxide (Ni, Cu, and Co) filter and a Soller slit assembly were placed in front of the detector to reduce the elastic scatter peak. Nine scans of a sample containing only sample buffer (50 mM $NaPO_4$, pH 7.2) were collected at each absorption edge, averaged, and subtracted from the averaged data for the protein samples to remove Z-1 K_β fluorescence and produce a flat preedge baseline. This procedure allowed data with an excellent signal-to-noise ratio to be collected down to 100 μM total copper in the sample. The samples (70 μL) were measured as aqueous glasses (>20% ethylene glycol) at 15 K. Energy calibration was achieved by reference to the first inflection point of a metal foil placed between the second and third ionization chamber. Data reduction and background subtraction were performed using the program modules of EXAFSPAK.[48] Data from each detector channel were inspected for glitches or drop outs before inclusion in the final average. Spectral simulation was carried out using the program EXCURVE 9.2,[49−52] as previously described,[53,54] or the OPT module of EXAFSPAK with the theoretical

(46) Ralle, M.; Lutsenko, S.; Blackburn, N. J. *J. Biol. Chem.* **2003**, *278*, 23163−23170.
(47) Nilges, M. J. Illinois EPR Research Center (IERC), University of Illinois: Urbana−Champaign, IL, 1979.
(48) George, G. N. Stanford Synchrotron Radiation Laboratory, Menlo Park, CA, 1990.

phase shifts and amplitude functions calculated by FEFF 8.0.[55] Both programs gave equivalent results.

Results

Recombinant *B. subtilis* Sco (BSco) lacking the first 19 amino-acid membrane-spanning domain was overexpressed in *E. coli* to produce a final construct of 174 amino acids. The translated gene sequence of the expressed truncated protein is shown in Figure 1. Metal reconstitution was performed by adding Cu(II), Zn(II), Ni(II), and Co(II) to the DTT-reduced apo protein at a 5:1 ratio of metal to protein, followed by exhaustive dialyses to remove nonbound metal, with all steps being carried out anaerobically. Under these conditions, copper, zinc, and nickel each bound at a 1:1 ratio. Co(II), on the other hand, did not bind in measurable amounts. When the apo protein was presented with a mixture of Cu(II), Zn(II), and Ni(II), Cu(II) was found to bind preferentially. In the presence of a 5-fold excess of all three metals, BSco-bound Cu(II) in a 1:1 ratio with essentially no binding of Zn(II) or Ni(II). Two methods were used to generate the Cu(I) form of BSco. The Cu(II)-reconstituted protein could be reduced to the Cu(I) form by anaerobic addition of dithionite. Alternatively, reconstitution could be achieved by addition of a small excess of $[(CH_3CN)_4Cu^I]PF_6$ to the reduced apo protein followed by exhaustive dialysis, as described previously.[46] This procedure routinely produced Cu(I)/protein ratios less than unity, with typical ratios around 0.7. Spin quantitation of the EPR spectra of the copper-loaded BSco samples showed that the Cu(II) form was 100% paramagnetic, whereas the Cu(I) forms were EPR silent. Analysis of the Ni(II) sample also gave an EPR silent species.

Cu^{I}BSco. Figure 2a,b shows XAS data on Cu(I)-loaded BSco. Figure 2a shows data for the form prepared by dithionite reduction of the Cu(II)-loaded protein, and Figure 2b shows data for the form prepared by $[(CH_3CN)_4Cu^I]PF_6$ reconstitution of the reduced apo protein. The data are similar but not identical. The best fits to the EXAFS and Fourier transforms are given in Table 1. Because of the homology with yeast Sco1p, the initial strategy was to simulate the data with chemical models built from combinations of two cysteine and one histidine ligand donor sets. Because the NMR structure[41] showed that the potential N(histidine) ligand atoms were 11−15 Å from the thiol groups of the putative ligating cysteine residues, and would therefore require a large conformational change to enable them to coordinate to the Cu, we also tested models which included only S(Cys) coordination, or Cys + nonhistidine O/N scatterers. For the dithionite-reduced sample, the best fit was obtained with two Cu−S(Cys) interactions and a partially occupied shell of low-*Z* (O/N) scatterers. Fits with a single shell of two Cu−S scatterers exhibited Debye−Waller (DW) factors that were higher than is normally expected for a single shell, suggesting nonequivalence of the Cu−S interactions. Fits with more reasonable DW factors could be obtained by splitting the Cu−S shell into two components with individual distances of 2.18 and 2.27 Å, respectively, but the observed splitting was below the limit of the resolution of the data; $\Delta R = \pi/2\Delta k = 0.14$ Å for data with a *k*-range of 2−13 Å^{-1}. When data to $k = 15$ Å were simulated, fits with a split Cu−S shell were no better than those with a single Cu−S shell. In all cases, the fit was improved by including a low-*Z* (O/N) scatterer at 2.01 Å. However, including the outer-shell scattering from imidazole ring C and N atoms produced neither quantitative nor qualitative (visual) improvements in the fit. Our results suggest that the Cu^{I}BSco is coordinated by two cysteine residues with a third O/N ligand. Our data is more consistent with this third ligand being derived

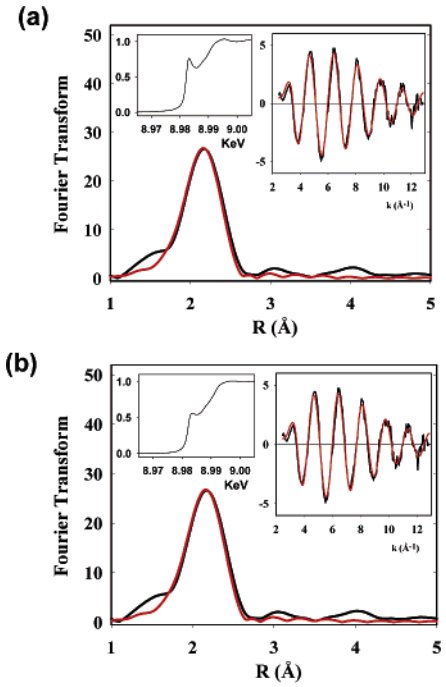

Figure 2. XAS of Cu^{I}BSco. Experimental (black) and simulated (red) Fourier transforms (phase corrected) and EXAFS (inset, right) are plotted for (a) dithionite-reduced (fit C, Table 1) and (b) $[(CH_3CN)_4Cu^I]PF_6$-reconstituted proteins (fit F, Table 1). The absorption edges for each derivative are also shown as insets (left).

Table 1. Fits Obtained to the EXAFS of the Cu(I)-Loaded BSco by Curve Fitting Using the Program EXCURV 9.2

		Cu–S			C–N(His)[b]			Cu–N/O			
fit	*F*[a]	no.[c]	*R* (Å)[d]	DW (Å^2)	no.[c]	*R* (Å)[d]	DW (Å^2)	no.[c]	*R* (Å)[d]	DW (Å^2)	$-E_0$
					Dithionite-Reduced Cu^{I}BSco						
A	0.520	2	2.219	0.010							2.61
B	0.345	2	2.233	0.012	1	2.040	0.012				6.78
C	0.291	2	2.228	0.010				0.5	1.951	0.005	4.42
D	0.287	1	2.179	0.005				0.5	1.944	0.005	4.37
		1	2.270	0.005							
					Cu(I)-Reconstituted Cu^{I}BSco						
E	0.224	2	2.219	0.011	1	1.972	0.009				2.88
F	0.246	2	2.221	0.011				1	1.975	0.009	3.02
G	0.232	1	2.157	0.005				1	1.991	0.012	3.02
		1	2.269	0.003							

[a] *F* is a least-squares fitting parameter, defined as $F^2 = (1/N)\sum_{i=1}^{N} k^6(\text{data} - \text{model})^2$. [b] Fits modeled histidine coordination by an imidazole ring, which included single and multiple scattering contributions from the second shell (C2/C5) and third shell (C3/N4) atoms, respectively. [c] Coordination numbers are generally considered accurate to ±25%. [d] In any one fit, the statistical error in bond lengths is ±0.005 Å. However, when errors due to imperfect background subtraction, phase-shift calculations, and noise in the data are compounded, the actual error is probably closer to ±0.02 Å.

(49) Binsted, N.; Gurman, S. J.; Campbell, J. W. EXCURVE, 9.2 ed.; Daresbury Laboratory: Warrington, England, 1998.
(50) Gurman, S. J.; Binsted, N.; Ross, I. *J. Phys. C* **1984**, *17*, 143−151.
(51) Gurman, S. J.; Binsted, N.; Ross, I. *J. Phys. C* **1986**, *19*, 1845−1861.
(52) Binsted, N.; Hasnain, S. S. *J. Synchrotron Rad.* **1996**, *3*, 185−196.
(53) Ralle, M.; Berry, S. M.; Nilges, M. J.; Gieselman, M. D.; van der Donk, W. A.; Lu, Y.; Blackburn, N. J. *J. Am. Chem. Soc.* **2004**, *126*, 7244−7256.
(54) Blackburn, N. J.; Rhames, F. C.; Ralle, M.; Jaron, S. *J. Biol. Inorg. Chem.* **2000**, *5*, 341−353.
(55) Zabinsky, S. I.; Rehr, J. J.; Ankudinov, A. L.; Albers, R. C.; Eller, M. J. *Phys. Rev. B* **1995**, *52*, 2995−3009.

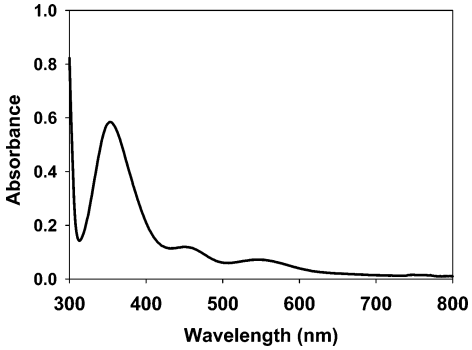

Figure 3. UV/vis spectrum of Cu^{II}BSco.

from a nonhistidine O/N scatterer, from a solvent, or from an additional protein residue, but does not exclude partial shell occupancy by a histidine residue.

When BSco was loaded with Cu(I) by reconstitution of the apo protein with $[Cu^{I}(CH_3)_4]PF_6$, similar but not identical results were obtained and listed as fits E and F in Table 1. EXAFS simulations gave equivalent fits to the dithionite-reduced data, with the difference that the O/N shell exhibited a lower DW factor, which was now within the range ($2\sigma^2 = 0.002-0.010$ Å^2) expected for a single scatterer. The data were fit equally well with or without the imidazole outer-shell scattering. Therefore, simulation of the EXAFS data provided no evidence for or against histidine as a ligand to Cu(I).

A more significant difference was seen in the intensity of the 8983 eV edge feature. This feature is due to the 1s → 4p transition and is most intense when the excited state orbitals are purely p in character. Mixing of s character into these orbitals lowers the intensity of the transition and can occur by increased coordination number, lowering of the symmetry, or metal−ligand covalency.[56−59] In the present case, the intensity of the 8983 eV feature is typical of a 3-coordinate Cu−S system and thus supports the conclusions drawn from analysis of the EXAFS. However, the intensity of the reconstituted sample is less than that of the dithionite-reduced sample, suggesting some difference in the Cu(I) coordination. Given the evidence for nonstoichiometric coordination of a third ligand in the dithionite-reduced sample, it seems likely that the site partitions between 2-coordinate CuS_2 and 3-coordinate $CuS_2(N/O)$ species. The data suggest that more of the 3-coordinate species exists in the Cu(I)-reconstituted sample. The presence of acetonitrile during the reconstitution process is a potential source of an additional coordinating ligand and may argue that the third ligand is more likely to be exogenous than a protein-derived residue in both forms of the Cu(I)-loaded BSco.

Cu^{II}BSco. A. UV/Vis Spectroscopy. Cu(II)-reconstituted BSco is reddish-orange in color. The UV/vis spectrum (Figure 3) features a major absorption band at 354 nm, $\epsilon = 4700$ cm^{-1} M^{-1}, and two minor absorption bands at 455 and 560 nm responsible for the red color of the protein solution. The intense absorption at 354 nm is likely due to thiolate−Cu(II) charge transfer. When Cu^{II}BSco was reduced by 20 mM sodium dithionite under anaerobic conditions, the sample was rapidly bleached to a colorless solution.

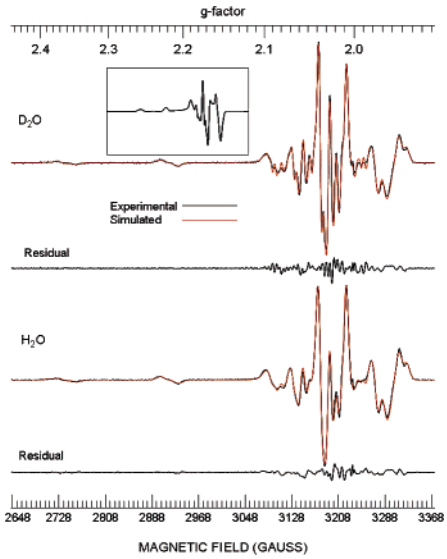

Figure 4. Experimental (black) and simulated (red) second-derivative X-band (9.055 GHz) EPR spectra of Cu^{II}BSco in H_2O and D_2O. The inset shows the first-derivative spectrum.

B. EPR, ENDOR, and ESEEM Spectroscopy. The X-band EPR of Cu^{II}BSco (Figure 4) gives a nearly axial copper spectrum with $g_{\|} = 2.15$, $g_{\perp} = 2.03$, and well-resolved ^{63,65}Cu hyperfine splittings. Second-derivative spectra show the presence of a resolved ligand superhyperfine structure that can be fitted by inclusion of nitrogen and/or proton splittings. Simulations show that this structure can be best accounted for with the hyperfine coupling of two spins, one ^{14}N ($I = 1$) and one proton ($I = {}^1/_2$), with the simulation parameters in Table 2.[61] A more simplified spectrum is seen at Q-band (Figure 5), with the ^{63,65}Cu splitting of the parallel component ($A_z = 180$ G) being clearly observed. At Q-band frequencies, the rhombic splitting due to g is partially resolved in the second-derivative spectrum.[62] For the simulations of the second-derivative X- and Q-band spectra, only a single species was necessary to reproduce all of the features in the spectrum.[63]

The X-band EPR spectrum of Cu^{II}BSco shows significant line narrowing when the sample is exchanged with D_2O. The decrease in line width is most noticeable along the x direction, where it decreases from 6.9 to 4.7 G (Table 2).[64] (See further discussion in the Supporting Information.)

(56) Kau, L. S.; Spira-Solomon, D.; Penner-Hahn, J. E.; Hodgson, K. O.; Solomon, E. I. *J. Am. Chem. Soc.* **1987**, *109*, 6433−6422.
(57) Blackburn, N. J.; Strange, R. W.; Reedijk, J.; Volbeda, A.; Farooq, A.; Karlin, K. D.; Zubieta, J. *Inorg. Chem.* **1989**, *28*, 1349−1357.
(58) Pickering, I. J.; George, G. N.; Dameron, C. T.; Kurz, B.; Winge, D. R.; Dance, I. G. *J. Am. Chem. Soc.* **1993**, *115*, 9498−9505.
(59) Ralle, M.; Lutsenko, S.; Blackburn, N. J. *J. Inorg. Biochem.* **2004**, *98*, 765−779.
(60) Rose, M. E. *Elementary Theory of Angular Momentum*; Wiley: New York, 1957.
(61) The simulations include the contribution to both naturally occurring copper nuclear isotopes, ^{63}Cu and ^{65}Cu, as the isotope splitting can be resolved in the parallel features of the X-band spectrum.
(62) Because the rhombic splitting in g of 32 G is competitive with the superhyperfine splitting from the nitrogen, the rhombic splitting in g cannot be accurately measured directly from the Q-band spectrum without the aid of spectral simulation.
(63) For the first-derivative X-band and Q-band spectra, the simulations showed the presence of a second axial species with very broad line widths, no resolved hyperfine structure, g values of 2.12 for $g_{\|}$ and 2.06 for $g_{\perp}$, and a weighting of 10−15%. This minor component is possibly due to dimerization and/or clustering and does not necessarily represent a second species. The parallel g and A parameters reported here are similar to those for one of the two species that are observed by Balatri and co-workers: Balatri, E.; Banci, L.; Bertini, I.; Cantini, F.; Ciofi-Baffoni, S. *Structure* **2003**, *11*, 1431−1443.
(64) The effect of D_2O exchange was also seen in the Q-band spectrum, but the effect was much smaller because the spectra are not as well resolved as those for the X-band.

Table 2. EPR Spin Hamiltonian and Strain Parameters for Cu^{II}BSco Obtained from Simulation of CW EPR Spectra[a]

g_x	2.0343	σg_x	+0.0009	[+0.028]
g_y	2.0289	σg_y	+0.0009	[+0.035]
g_z	2.1501	σg_z	+0.0029	[+0.020]
(Cu)A_x[b]	−124.6	σA_x	+1.5	[−0.012]
(Cu)A_y	−109.2	σA_y	−3.9	[+0.036]
(Cu)A_z	−533.1	σA_z	−0.5	[+0.001]
α_{gA}[c]	+13.4°			
β_{gA}	+1.2°			
γ_{gA}	+12.0°			
(Cu)QD[b]	+4.8			
(Cu)QE	−2.6			
W_x[d]	4.7	W_x[e]	6.9	
W_y	7.2	W_y	7.7	
W_z	9.6	W_z	9.7	
(N)A_x	30.6	α_{gA}	107°	
(N)A_y	41.1	β_{gA}	15°	
(N)A_z	30.8	γ_{gA}	−90°	
(H1)A_x	20.9	α_{gA}	39°	
(H1)A_y	16.3	β_{gA}	21°	
(H1)A_z	18.4	γ_{gA}	0°	

[a] Hyperfine principal values in MHz. (For units of 10^{-4} cm^{-1}, divide by 3.) Fractional strain is given in square brackets (for g, $\Delta(\Delta g)/\Delta g$ is given); the sign in front of the variance in the principal values of g and A represents the correlation coefficient of ±1.0. nd = not determined. [b] Hyperfine and nuclear quadrupole values are for ^{63}Cu. $A(^{65}Cu) = A(^{63}Cu)*1.0713$ and $QD(^{65}Cu) = QD(^{63}Cu)*0.878$, $QE(^{65}Cu)* = QE(^{63}Cu)*0.878$. [c] Euler angles (convention of Rose[60]) relating the noncoincidence between the copper g and A (nuclear quadrupole tensor is assumed coincident with A). [d] Residual line width (Gaussian) in Gauss for D_2O. [e] Residual line width (Gaussian) in Gauss for H_2O

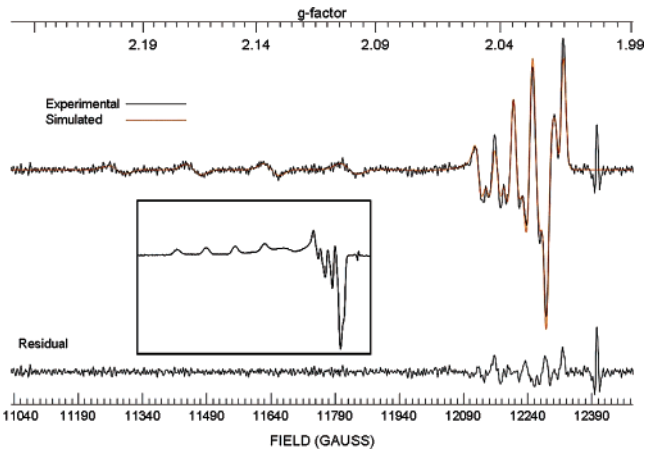

Figure 5. Experimental (black) and simulated (red) second-derivative Q-band (34.76 GHz) EPR spectra of Cu^{II}BSco in H_2O. The inset shows the first-derivative spectrum. The sharp signal at $g = 2.000$ is due to the quartz tube.

C. ENDOR Spectroscopy. The ^{14}N and ^{1}H hyperfine interactions determined from simulation of the continuous wave (CW) EPR data account for a single nitrogen and a single proton. To confirm our analysis and to identify more weakly coupled nuclei which could reveal the identity and symmetry of the ligands in the Cu^{II}BSco complex, we have carried out ENDOR experiments. Figure 6 shows the pulsed ENDOR spectra of Cu^{II}-BSco for various values of the length of the first π pulse; the magnetic field was set to the high-field maximum of the spectra which is nominally $g = 2.022$. The most prominent features are (i) a pair of lines split by 19 MHz and centered around the proton resonance frequency and (ii) a peak centered at 17 MHz. For most protons, half the hyperfine splitting is smaller than

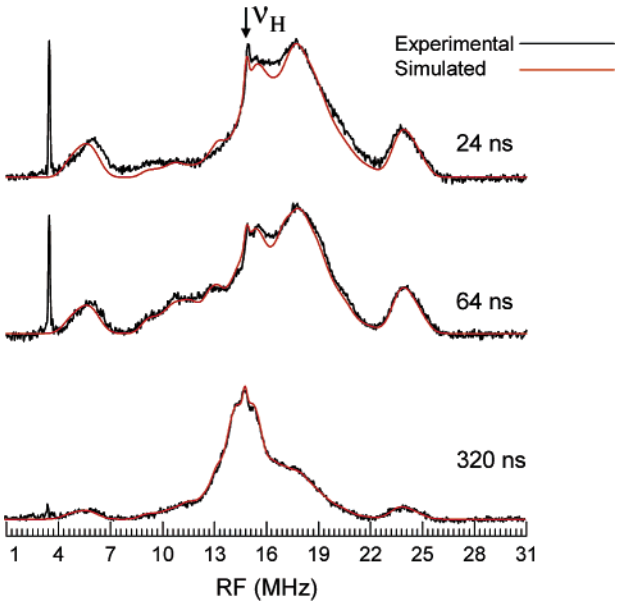

Figure 6. Experimental (black) and simulated (red) X-band (9.67 GHz) ENDOR spectra of Cu^{II}BSco in H_2O at various values of the π pulse. The magnetic field was set at 3489 G.

the nuclear Zeeman interaction and a pair of lines separated by the hyperfine splitting and centered at the proton resonance is expected. For nuclei such as ^{14}N, which has a small nuclear Zeeman term, a pair of lines split by twice the nuclear Zeeman frequency and centered at half the hyperfine splitting is expected. Further, this pair of lines is split again by the nuclear quadrupole term. The resonance at 17 MHz can be assigned to a ^{14}N having an isotropic splitting of 34 MHz.

As the pulse length is shortened, the pulses become less selective and nuclei with small hyperfine splittings are suppressed so that the ^{14}N resonance(s) at 17 MHz are better seen. For $t_\pi = 64$ ns, other peaks are seen corresponding to the low-frequency branch of proton resonances having hyperfine splittings between 5 and 12 MHz, and for $t_\pi = 320$ ns, a pair of lines are seen corresponding to a proton splitting of around 3 MHz.

The ENDOR spectrum of Cu^{II}BSco in D_2O with $t_\pi = 64$ ns is essentially identical to that in H_2O, demonstrating that none of the large proton splittings are due to exchangeable protons (Figure S1, Supporting Information). Some differences are seen with $t_\pi = 320$ ns, and these correspond to a loss of intensity corresponding to a splitting with $A_\perp$ of 3.5 MHz for an exchangeable proton.

To better quantify the smaller proton splittings as well as the proton splitting of 19 MHz and the nitrogen resonance at 34 MHz, simulations were performed. By allowing for anisotropy in the hyperfine splittings, reasonable fits could be obtained for both the H_2O and D_2O spectra if five proton splittings, as listed in Table 3, were used. Three protons, H1, H2, and H3, have fairly isotropic tensors with isotropic splittings of 18.5, 8.4, and 5.1 MHz, respectively (Table 3). The other two protons, Hex (exchangeable)[65] and Hrem (remote),[66] have smaller and more anisotropic splittings.[67]

(65) Simulation of the CW EPR spectrum in H_2O using the line widths used in simulating the D_2O spectrum and assuming two equivalent protons gives proton couplings of 4.8, 7.2, and 9.6 MHz for A_x, A_y, and A_z. These splittings are larger than those obtained from ENDOR and may represent additional broadening from more distant or matrix solvent molecules.

Table 3. Spin Hamiltonian Parameters for Cu^{II}BSco Obtained from Simulation of ENDOR Spectra[a]

						intensity weighting at pulse length (ns)		
	A_x	A_y	A_z	A_{iso}	W^b	320	64	24
N1[c,d]	33.58	41.39	30.22	35.06	1.01	1.00	1.00	1.00
H1[c]	20.72	17.98	16.66	18.45	0.88	0.81	0.98	0.73
H2[e]	5.43	7.81	12.02	8.42	0.70	1.04	1.06	0.34
H3[f]	7.30	4.00	4.00	5.10	0.65	1.23	0.52	0.05
Hex[f]	1.30	−3.50	−3.50	−1.90	0.50	1.08	0.35	0.11
Hrem[f]	3.55	−1.55	−1.55	−0.15	0.75	4.05	0.40	0.08

[a] Isotropic and principal hyperfine values in MHz. [b] Line width in MHz (Gaussian peak-to-peak). [c] Euler angles as from CW simulations (Table 3). [d] $QD = -1.42$ and $QE = 0.09$. The Euler angles for Q are assumed coincident with A. [e] $\beta \approx 30°$. [f] Assignment of A_x vs A_y is arbitrary.

Comparison of values in Tables 2 and 3 shows very good agreement between EPR and ENDOR results for the hyperfine tensor of the nitrogen and the H1. For the most part, the values are in agreement with experimental error (1 MHz for EPR and 0.5 MHz for ENDOR). Although the values from ENDOR should be more accurate, the overlap from the partially suppressed proton peaks as well as the broad line widths and unresolved splitting due to the nuclear quadrupole coupling limits the accuracy of the ENDOR measurements for the nitrogen.

ENDOR spectra show the presence of only one unique nitrogen and could be fitted with a nitrogen/H1 proton intensity ratio of 1:1 (Table 3). This is consistent with and supports the results of the simulations of the CW spectra. It is possible that observed splittings in the CW spectrum correspond to two equivalent nuclei. Simulations of the CW EPR spectra, in particular the X-band D_2O spectrum, which has the best resolution, were repeated with two nitrogens (Figure S2, Supporting Information) and/or two protons. The observed spectra could not be fit in any way with two equivalent nitrogens. The spectra also could not be fit using two equivalent protons, but a second inequivalent proton could be included if the splitting was around 5−12 MHz. These values are in agreement with the splittings for H2 determined from ENDOR spectra.

D. ESEEM Spectroscopy. Although ENDOR spectra give a good account of coupling to nearby nuclei, ESEEM can be used to explore couplings to more remote nuclei, especially nitrogens. Figure 7 shows two slices from a two-dimensional three-pulse ESEEM experiment. The top spectrum ($\tau = 304$ ns slice) shows peaks at 0.73, 1.6, and 4.0 MHz, which are characteristic of the remote nitrogen of a copper-coordinated imidazole.[68] Also seen in the two-dimensional ESEEM spectra are sharp peaks at 2.19 and 2.93 MHz, which can be clearly seen in the middle spectrum ($\tau = 384$ ns slice) of Figure 7. These peaks have been attributed to a backbone nitrogen, in particular that of the copper-bound cysteine.[69] These two peaks along with the peak at 0.73 MHz form a set of three pure quadrupole transitions and are consistent with a $|e^2qQ|$ of 3.4 MHz and an η of 0.44 (see Supporting Information). A double quantum transition is also expected for the backbone nitrogen(s) around 4 MHz[69] and, as such, will overlap with the double quantum transition for the histidine.[70] The peak at 0.73 MHz is due to at least three different pure quadrupole transitions, which is why it is the most intense peak in the spectrum. Also noticeable in the projection spectrum is that the peaks for the backbone nitrogens at 2.2 and 2.9 MHz are about twice as intense as the 1.6 MHz histidine peak and half as intense as the 0.73 MHz peak. This 4:1:2:2 ratio is consistent with a cysteine/histidine ratio of 2:1.

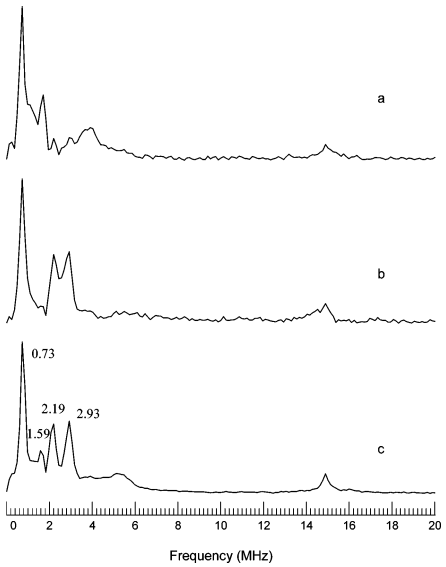

Figure 7. Two-dimensional T vs τ three-pulse ESEEM spectra of Cu^{II}-BSco in H_2O for $t_\pi = 32$ ns: (a) $\tau = 304$ ns; (b) $\tau = 384$ ns; (c) projection along T.

Table 4. Fits Obtained to the EXAFS of the Cu^{II}BSco by Curve Fitting Using the Program EXCURV 9.2

		Cu–S			C–N(His)[b]			Cu–N/O			
fit	F^a	no.[c]	R (Å)[d]	DW (Å^2)	no.[c]	R (Å)[d]	DW (Å^2)	no.[c]	R (Å)[d]	DW (Å^2)	$-E_0$
A	0.558	2	2.188	0.014	1	1.909	0.002				1.07
B	0.289	2	2.211	0.018	1	1.948	0.011	1	1.948	0.011	1.19
C	0.204	2	2.216	0.018	2	1.947	0.010				1.50
D	0.210	1	2.151	0.007	2	1.938	0.012				1.10
		1	2.276	0.007							

[a] F is a least-squares fitting parameter defined as $F^2 = (1/N)\sum_{i=1}^{N} k^6(\text{data} - \text{model})^2$. [b] Fits modeled histidine coordination by an imidazole ring, which included single and multiple scattering contributions from the second shell (C2/C5) and third shell (C3/N4) atoms, respectively. [c] Coordination numbers are generally considered accurate to ±25%. [d] In any one fit, the statistical error in bond lengths is ±0.005 Å. However, when errors due to imperfect background subtraction, phase-shift calculations, and noise in the data are compounded, the actual error is probably closer to ±0.02 Å.

E. EXAFS. The EXAFS of Cu^{II}BSco was simulated using an approach similar to that of the Cu(I)-loaded form. Table 4 lists a number of fits generated using different chemical models of Cu(II) coordination. We first tested a simple 3-coordinate model involving two Cu−S(Cys) and one Cu−N(His) which would correspond to the minimal number of ligands consistent with ENDOR and ESEEM and the EXAFS of the Cu^{I}BSco. Because of the known preference of Cu(II) for coordination numbers of 4 and higher, we introduced next additional low-Z scatterers, either as imidazoles from histidine or as isolated O/N

(66) The Hrem contribution makes a relatively large contribution to the $t_\pi = 320$ ns spectrum signal and is probably due to more than one type of weakly coupled (remote) proton.
(67) A sharp peak at 3.46 MHz is observed in concert with the copper EPR signal, which we cannot assign at this time.
(68) Mims, W. B.; Peisach, J. *J. Chem. Phys.* **1978**, *69*, 4291−4930.
(69) van Gastel, M.; Coremans, J. W. A.; Jeuken, L. J. C.; Canters, G. W.; Groenen, E. J. J. *J. Phys. Chem. A* **1998**, *102*, 4462−4470.
(70) Because of the overlap between peaks from the histidine and backbone nitrogens, the presence of combination peaks, which could arise from the presence of more than one histidine nitrogen, could not be determined.

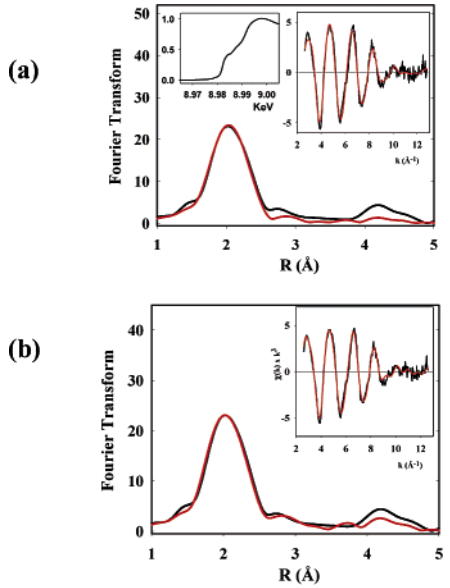

Figure 8. Experimental (black) and simulated (red) Fourier transforms (phase corrected) and EXAFS (inset, right) for Cu^{II}BSco. (a) Two Cu−S, one Cu−His, and one Cu−N/O (fit B, Table 4). (b) Two Cu−S and two Cu−His (fit C, Table 4). The absorption edge is also shown in the left inset of the top panel.

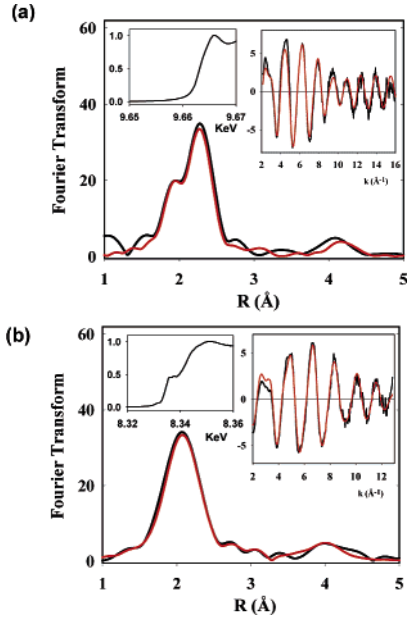

Figure 9. Experimental (black) and simulated (red) Fourier transforms (phase corrected) and EXAFS (inset, right) for (a) Zn^{II}BSco (fit B, Table 5) and (b) Ni^{II}BSco (fit D, Table 5). The absorption edge is shown in the left inset for each metal complex.

(solvent) scatterers. The results are listed in Table 4, fits A−D. The simple 3-coordinate model produced an inferior fit compared to that of 4-coordinate models. The best fit was obtained with two Cu−S and two Cu−N(His) interactions (Table 4, fit C), and the fit with two Cu−S, one Cu−N(His), and one Cu−O/N (nonhistidine) was worse by a factor of 40% (Table 4, fit B). Similar to Cu^{I}BSco, the Cu−S shell exhibited a high DW factor, suggestive of structural disorder. We therefore tested whether the data could tolerate a split Cu−S shell. A good fit was obtained (Table 4, fit D) with two different Cu−S interactions at 2.15 and 2.28 Å, respectively, but splitting the Cu−S shell in this way did not improve the *F* value. However, these simulations decreased the DW factor from the unreasonably high value of $2\sigma^2 = 0.018$ Å^{-1} for the unsplit Cu−S shell to a more chemically reasonable value of $2\sigma^2 = 0.007$ Å^{-1} for the split Cu−S shell. Therefore, the EXAFS is not inconsistent with differing Cu−S interactions but provides only weak evidence in support of a split shell. Although the two His model was quantitatively superior to the one His, one O/N model, care must be used when choosing between His and non-His scatterers because these can only be distinguished by their contributions to the extremely weak outer-shell peaks around 3 and 4 Å, which are often seriously impacted by the energy range in the *k* space and by noise in the data. Although NMR of the Cu(II) form showed that proton resonances assigned to two histidines (H55, H135, Figure 1) are broadened so that the $CuS_2(His)_2$ model is reasonable, evidence from EPR for a single N hyperfine coupling is more compelling. The experimental and simulated data for the $CuS_2(His)_2$ and $CuS_2(His)X$ (X = nonimidazole N/O) models are shown in Figure 8.

Zn^{II}BSco. The experimental and simulated EXAFS and Fourier transform (FT) for the Zn(II) derivative of BSco are shown in Figure 9a, with parameters used to fit the data listed in Table 5. The Zn EXAFS is of particular interest because it shows a resolved splitting of the first-shell FT peak into a low-*Z* (O/N) component at ∼2.0 Å and a Zn−S component at ∼2.3 Å (both values are phase corrected). This splitting is partially attributable to the increased range of the data ($k = 2-16$ Å^{-1}) but arises more from a larger metrical difference between the Zn−N/O and Zn−S shells of backscatterers. Simulations (Table 5, fits A and B) showed that two Zn−S interactions at 2.28 Å and two O/N ligands at 2.01 Å fit the data well and that the O/N shell was about equally well-fit by two histidines (fit A) or by one His and one non-His ligand. In contrast to the Cu(II) data, the Zn(II) data showed a small preference for the one histidine model. Also in contrast, the DW factors of both the Zn−S and Zn−O/N shells were much reduced, suggesting a more homogeneous Zn(II) site.

Ni^{II}Bsco. A. Electronic Spectrum. Ni^{II}BSco is pink. The optical spectrum (Figure 10) shows two weak bands at 540 and 360 nm which correlate with the two low-energy bands of the Cu(II) spectrum but are shifted to higher energy. The intense high-energy band seen at 350 nm in the Cu(II) derivative is either missing or, more likely, red shifted into the protein 280 nm band. In support of the latter premise, the absorbance at 280 nm increases more on Ni(II) loading than on Cu(II) loading. We did not attempt to investigate further the high-energy thiolate−metal charge-transfer (CT) band in the Ni(II) species. Such bands are generally observed at wavelengths below 300 nm in inorganic Ni^{II}−thiolate complexes.[71] The Ni(II) spectrum is similar to that reported previously for the bacterial Sco homologue PrrC.[72]

B. EXAFS Spectroscopy. The experimental and simulated EXAFS and FT for the Ni^{II}BSco is shown in Figure 9b, with the fitting parameters listed in Table 5, fits C and D. As in the Zn(II) derivative, a model involving two Ni−S and two O/N ligands fits the data well, with a small preference for one histidine over two histidine structures.

(71) Maroney, M. J.; Choudhury, S. B.; Bryngelson, P. A.; Mirza, S. A.; Sherrod, M. J. *Inorg. Chem.* **1996**, *35*, 1073−1076.
(72) McEwan, A. G.; Lewin, A.; Davy, S. L.; Boetzel, R.; Leech, A.; Walker, D.; Wood, T.; Moore, G. R. *FEBS Lett.* **2002**, *518*, 10−16.

Table 5. Fits Obtained to the EXAFS of the Zn(II)- and Ni(II)-Loaded BSco by Curve Fitting Using the Program EXCURV 9.2

		metal–S			metal–N(His)[b]			metal–N/O			
fit	F[a]	no.[c]	R (Å)[d]	DW (Å^2)	no.[c]	R (Å)[d]	DW (Å^2)	no.[c]	R (Å)[d]	DW (Å^2)	$-E_0$
					Zn^{II}BSco ($k = 2-16$)						
A	0.338	2	2.277	0.006	2	1.999	0.006				2.95
B	0.314	2	2.278	0.006	1	2.021	0.002	1	1.942	0.007	3.06
					Ni^{II}BSco ($k = 2-13$)						
C	0.373	2	2.186	0.011	2	1.991	0.014				5.80
D	0.282	2	2.178	0.010	1	1.942	0.003	1	2.085	0.004	6.78

[a] F is a least-squares fitting parameter defined as $F^2 = (1/N)\sum_{i=1}^{N} k^6(\text{data} - \text{model})^2$. [b] Fits modeled histidine coordination by an imidazole ring, which included single and multiple scattering contributions from the second shell (C2/C5) and third shell (C3/N4) atoms, respectively. [c] Coordination numbers are generally considered accurate to ±25%. [d] In any one fit, the statistical error in bond lengths is ±0.005 Å. However, when errors due to imperfect background subtraction, phase-shift calculations, and noise in the data are compounded, the actual error is probably closer to ±0.02 Å.

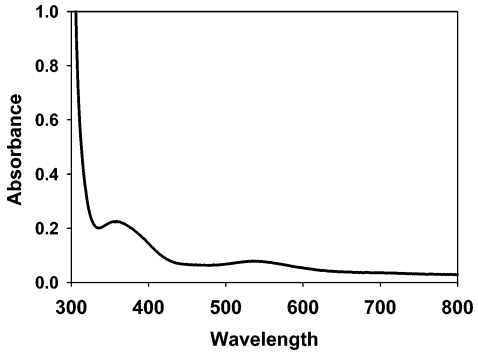

Figure 10. UV/vis spectrum of Ni^{II}BSco.

Discussion

We have used a number of spectroscopic techniques to investigate Cu, Zn, Ni, and Co binding by a soluble form of the *B. subtilis* Sco cytochrome oxidase assembly chaperone protein, produced as an untagged soluble construct by truncation of the N-terminal membrane-anchoring helix. The analogous protein from yeast, Sco1p, has been reported to bind a single Cu(I) per protein and has been identified as an accessory protein in COX assembly, specifically accepting Cu(I) from Cox17.[32,45] The PrrC homologue from *Rhodobacter sphaeroides* has also been reported to bind Cu(II) and Ni(II).[72] The existence of the Cu(II) complex has been noted previously,[41,72] but its properties or those of other metal-bound congeners were not explored in detail. Our data have established a 1:1 binding stoichiometry for Cu(II), Zn(II), and Ni(II) but no binding for Co(II). The reddish-orange Cu(II) form of the protein is reducible by dithionite to the colorless Cu(I) derivative which could be prepared directly by reconstitution with the Cu^I−acetonitrile complex, but this procedure always led to levels of Cu(I) binding (0.5−0.7) lower than those of reconstitution to the Cu(II) form.

Previous XAS characterization of Sco1p by Winge and coworkers established that Cu(I) was bound by two cysteines.[45] Subsequent mutagenesis identified C148 and C152 as probable candidates. H239 was also implicated as a ligand from mutagenesis, but inclusion as a Cu(I) ligand did not improve EXAFS fits. Our XAS data on the Cu(I) form of the bacterial Sco are in agreement with these predictions, where the corresponding residues are C45, C49, and H135. The metrical details of the samples produced by dithionite reconstitution or by direct reconstitution are similar and are comparable to those reported previously for Sco1p. Our analysis likewise fails to provide unambiguous evidence for histidine ligation. One minor difference between the two Cu(I) samples of this study is the absorption edge feature at 8983 eV which is more intense for the dithionite reduced form. The 8983 eV feature is well established as an accurate marker for coordination number and/or site symmetry. The intensity of this feature is inversely proportional to the coordination number, with linear 2-coordination exhibiting much more intensity than 3-coordination.[56−59] Although the intensity of the 8983 eV feature in Sco is typical of 3-coordinate species, the slight attenuation in the reconstituted sample may be the result of exogenous acetonitrile coordination by a subpopulation of molecules. Thus, we leave open the possibility that the Cu(I)-loaded BSco binds Cu(I) primarily via the two cysteine residues of the CXXXC motif, with weak association of a third ligand, X. It is possible that different forms of the protein partition among forms with X = H135, H55, water, buffer ion, or acetonitrile. The ability for bis-cysteinate Cu(I) centers in copper transporter chaperones to bind exogenous ligands has been reported previously.[46,59] Alternatively, at least some of these differences might arise as the result of the small (∼10%) population of molecules exhibiting the broad copper signal seen in the CW EPR spectrum.

The ability of BSco to form a stable Cu(II) complex is unusual among copper chaperones which are generally believed to transport copper in the Cu(I) form. The copper trafficking protein CopC from *Pseudomonas syringae* has been shown to bind copper in both oxidation states, but in this case, different binding sites were proposed.[73] The electronic spectrum of Cu(II) Sco shows two weak bands at 455 and 560 nm and a more intense band (ϵ = 4700 M^{-1} cm^{-1}) at 354 nm which can be assigned to a thiolate−Cu(II) charge-transfer transition. The extinction coefficient is more than twice that reported previously by Balatri et al. [41] on a heterogeneous Cu(II)-reconstituted form of BSco. The difference may be due to the smaller (>15%) population of the second Cu(II) species in our preparation in comparison to the earlier sample, where 50% of the copper was present in a different form. The UV/vis spectrum is typical of tetragonal type-2 Cu−thiolates where the Spσ transition (354 nm) is more intense than that of the Spπ and occurs at higher energy.[74−80] The high-energy Spσ interaction is dominant in tetragonal Cu^{II}−thiolates such as tet b and analogous complexes and occurs around 360−370 nm with extinctions of ∼5000 M^{-1} cm^{-1},[76,77] with weaker Sp$\pi \rightarrow Cu^{II}$ transitions to lower energy. The closest analogue of Cu(II) Sco is nitrosocyanin, the red

(73) Arnesano, F.; Banci, L.; Bertini, I.; Mangani, S.; Thompsett, A. R. *Proc. Natl. Acad. Sci. U.S.A.* **2003**, *100*, 3814−3819.
(74) Andrew, C. R.; Sanders-Loehr, J. *Acc. Chem. Res.* **1996**, *29*, 365−372.
(75) Solomon, E. I.; Szilagyi, R. K.; DeBeer George, S.; Basumallick, L. *Chem. Rev.* **2004**, *104*, 419−458.
(76) John, E.; Bharadwaj, P. K.; Potenza, J. A.; Schugar, H. J. *Inorg. Chem.* **1986**, *25*, 3065−3069.

cupredoxin protein from *Nitrosonomas europa*, which exhibits bands at 390, 496, and 720 of similar intensity to those in BSco.[78−81]

ENDOR spectra of Cu^{II}Bsco show the presence of a single ^{14}N coupling, and simulations of second-derivative CW EPR show that this coupling arises from only one nitrogen. The nearly isotropic ^{14}N coupling (A_{iso} of 35 MHz) is characteristic of that expected for copper−imidazole complexes. The value of A_{iso} is larger than that seen for type-1 complexes such as azurin (17 and 27 MHz[82]) but smaller than that seen for a square planar CuN_4 complexe such as $[Cu(imid)_4]^{2+}$ (40 MHz[83]). The EPR parameters of $g_{||} = 2.15$ and $A_{||} = 180$ G are similar to those of square planar N_2S_2 complexes.[84,85] However, these values are also expected to be consistent with a NS_2X complex, where X is an oxygenic ligand.

For a square planar NS_2X copper complex, the four ligands are expected to have their metal−ligand bonds oriented close to the lobes of the ground-state $d_{x^2-y^2}$ orbital. The smaller the angle between the Cu−N bond and a lobe of the $d_{x^2-y^2}$ orbital, the greater the spin density on the N will be.[86] The value of A_{iso} (35 MHz) and the orientation of the major component of the ^{14}N hyperfine tensor lying close (18°) to the g_y axis are consistent with the Cu−N bond being close to one of the lobes of the $d_{x^2-y^2}$ orbital.

The two cysteines should lie along two other lobes of the $d_{x^2-y^2}$ orbital and would be expected to have similar values of spin density and give rise to four approximately equal β-methylene splittings. Analysis of ENDOR spectra shows large couplings assignable to one cysteine, and for this cysteine, the two β-methylene protons are markedly inequivalent. This inequivalence suggests that one of the Cys ligands in BSco must lie somewhat between the lobes of the $d_{x^2-y^2}$ orbital but with suboptimal orientation of the cysteine with respect to the Cu $d_{x^2-y^2}$ orbital for pπ bond formation. Assuming the pπ orbital lies perpendicular to the Cu−S−C_β plane as it does in type-1 complexes, we estimate the Cu−S−C_β−H_β dihedral angles to be 79° and −41°, respectively.[87] The second cysteine is likely coordinated in a more optimal orientation for square planar geometry, giving rise to a strong Cu−S pσ bond where the β-methylene couplings are expected to be anisotropic and relatively small. The data are thus consistent with the Cu−N bond and one Cu−S bond lying close to the lobes of the $d_{x^2-y^2}$ orbital, whereas the other Cu−S bond lies off axis somewhere between the lobe of the $d_{x^2-y^2}$ orbital and the bisector between the lobes of the $d_{x^2-y^2}$ orbital.

CW EPR spectra in D_2O show that the copper site is accessible to solvent molecules. ENDOR spectra also show the presence of an exchangeable proton, presumably from an OH^-/H_2O. From the proton splittings, the Cu−H can be estimated as 3.7 Å (see Supporting Information). This distance is too long to place the OH^-/H_2O molecule as the fourth planar ligand and suggests that solvent may occupy an axial position.

The EXAFS data of the Cu^{II}BSco can be simulated by a 4-coordinate site composed of two Cu−S and two Cu−N/O scatterers. Axially coordinated solvent species are generally undetectable by EXAFS because of extremely high DW factors. The Cu−S distance of 2.21 Å is not as short as that found in native cupredoxins such as azurin, where the trigonal planar blue copper Cu−S distance is 2.14−2.16 Å[88−90] but is shorter than typical type-2 Cu−S distances.[91] However, EXAFS analysis may suggest that this shorter distance is a composite of a normal Cu−S distance of 2.27 Å and a short cupredoxin-like Cu−S distance of 2.15 Å (Table 4, fit D). Although EXAFS analysis is more compatible with two histidine ligands, distinguishing between N(His) and non-His O/N ligation can only be done by analysis of outer-shell scattering, which is weak and can be significantly impacted by noise in the data or by the small amount of adventitiously bound copper. The presence of couplings from only one N in the EPR and ENDOR argues against the two His model and supports an O scatterer as the origin of the fourth ligand. Lack of a strongly coupled exchangeable proton rules out equatorial water. Thus, when the EXAFS, EPR, and ENDOR data are considered together, it seems probable that the Cu(II) coordination in oxidized Cu^{II}-BSco can be approximated by a distorted tetragonal structure with equatorial ligation to a histidine and cysteine (more typical of square planar N_2S_2 complexes), a second cysteine having a pπ bond (but weaker than that in type-1 complexes), and a fourth O/N ligand which could be a histidine but is more likely to be an oxygenic endogenous ligand. Such a structure would require a geometry that is nominally square planar (tetragonal), yet with significant distortion (Figure 11). A weakly bound axial water ligand is probably also present. Although there appears to be significant structural asymmetry in the Cu−S bonds, with evidence for one short and one long Cu−S interaction, the electronic origin of this is probably quite different from the cupredoxin site and the shorter Cu−S most likely exhibits a type-2 Cu−S(pσ) interaction.

The EXAFS data for the Zn and Ni complexes of BSco provide further insight into the structure and selectivity of the metal binding site. The Zn−S distance of 2.28 Å is typical of 4-coordinate tetrahedral $ZnS_2(N/O)_2$ complexes.[92] The average

(77) Stibrany, R. T.; Fikar, R.; Brader, M.; Potenza, M. N.; Potenza, J. A.; Schugar, H. J. *Inorg. Chem.* **2002**, *41*, 5203−5215.
(78) Basumallick, L.; Sarangi, R.; DeBeer George, S.; Elmore, B.; Hooper, A. B.; Hedman, B.; Hodgson, K. O.; Solomon, E. I. *J. Am. Chem. Soc.* **2005**, *127*, 3531−3544.
(79) Arciero, D. M.; Pierce, B. S.; Hendrich, M. P.; Hooper, A. B. *Biochemistry* **2002**, *41*, 1703−1709.
(80) Lieberman, R. L.; Arciero, D. M.; Hooper, A. B.; Rosenzweig, A. C. *Biochemistry* **2001**, *40*, 5674−5681.
(81) The Cu(II) site in nitrosocyanin is best described as a square pyramid with one Cys, two His, and a water in the basal plane and a carboxylate O from Glu in an axial position. Detailed electronic structural analysis has assigned the 390 and 496 nm bands to the Cu−S(σ) and Cu−S(π) components, respectively, where the reversal in the relative intensities as compared to blue copper sites originates from the increase to 5-coordination accompanied by a rotation of the $d_{x^2-y^2}$ orbital relative to the Cu−S axis. Basumallick, L.; Sarangi, R.; DeBeer George, S.; Elmore, B.; Hooper, A. B.; Hedman, B.; Hodgson, K. O.; Solomon, E. I. *J. Am. Chem. Soc.* **2005**, *127*, 3531−3544.
(82) Werst, D. E.; Davoust, C. E.; Hoffman, B. M. *J. Am. Chem. Soc.* **1991**, *113*, 1533−1538.
(83) Van Camp, H. L.; Sands, R. H.; Fee, J. A. *J. Chem. Phys.* **1981**, *75*, 2098−2107.
(84) Blumberg, W. E.; Peisach, J. *J. Chem. Phys.* **1968**, *49*, 1793−1802.
(85) Myamoto, R.; Ohba, Y.; Iwaizumi, M. *Inorg. Chem.* **1990**, *29*, 3234−3238.
(86) On the basis of the value of 0.09 for ρN (the nitrogen spin density) for $[Cu(imid)_4]^{2+}$ (Werst, D. E.; Davoust, C. E.; Hoffman, B. M. *J. Am. Chem. Soc.* **1991**, *113*, 1533−1538), we estimate ρN to be 0.07 for Cu^{II}BSco.
(87) Full details of the assignment and analysis of hyperfine couplings are included as Supporting Information.
(88) Cheung, K. C.; Strange, R. W.; Hasnain, S. S. *Acta Crystallogr., Sect. D* **2000**, *56*, 697−704.
(89) DeBeer George, S.; Basumallick, L.; Szilagyi, R. K.; Randall, D. W.; Hill, M. G.; Nersissian, A. M.; Valentine, J. S.; Hedman, B.; Hodgson, K. O.; Solomon, E. I. *J. Am. Chem. Soc.* **2003**, *125*, 11314−11328.
(90) Berry, S. M.; Ralle, M.; Low, D. W.; Blackburn, N. J.; Lu, Y. *J. Am. Chem. Soc.* **2003**, *125*, 8760−8768.
(91) The average Cu−S distance for 4-coordinate $Cu^{II}S_2N_2$ complexes in the Cambridge database is 2.23 Å (average of 13 structures).

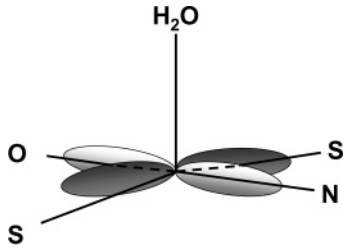

Figure 11. Orientation of the ligands to Cu(II) in BSco relative to the direction of the $d_{x^2-y^2}$ orbital, as suggested by analysis of EPR and ENDOR spectra.

Zn−S distance is largely unaffected by substituting O for N in one of the low-*Z* scatterers, although few examples of mixed $Zn-S_2ON$ coordination exist. Examples of $Zn(Cys)_2(His)_2$ are common in zinc finger motifs,[93] and ZnS_2NO coordination is also well documented in zinc methyl transferase enzymes such as methionine synthase[94,95] and farnesyl transferase in the presence of thiol substrates.[96] For Ni, the EXAFS derived Ni−S bond length of 2.19 Å is typical of Ni−S interactions in square planar NiS_2N_2 complexes found in the Cambridge database but is significantly shorter than the value found in tetrahedral Ni(II) complexes, which typically is around 2.24 Å.[97] Planar Ni^{II}−thiolates exhibit thiolate−Ni^{II} CT bands at higher energies than their Cu(II) homologues,[71] and it is likely that the ligand-to-metal charge-transfer (LMCT) band is obscured by the protein 280 nm absorption. The observed Ni−S bond length and the lack of EPR signal is therefore suggestive of square planar Ni(II) in the NiBSco. If we assume that the Zn(II) complex adopts tetrahedral geometry, it is apparent that either a variety of geometries is available to accommodate metal ion binding to BSco or that different coordinating residues are chosen by different metal ions. The reduced Ni(II) form of NiSOD has recently been shown to be coordinated by two cysteines and two peptide amide groups,[98,99] which leaves open the question of whether the NiBSco complex might differ from the Cu(II) complex and include coordination to the peptide backbone.

The absorption edge of the NiBSco is unusual. Two transitions appear on the rising edge at 8335.96 and 8337.74 eV. Although the latter transition is in the range reported for the $1s \rightarrow 4p_z$ transition expected for a square planar Ni(II) center,[100] the lower energy transition is atypical of Ni(II) complexes and would be more characteristic of a Ni(I) state. The absence of an EPR spectrum argues against an equilibrium mixture of Ni(I) and Ni(II), although photoreduction in the beam cannot be excluded.

Acknowledgment. The work was supported by grant GM54803 from the National Institutes of Health to N.J.B. The Illinois EPR Center is supported by the University of Illinois. We gratefully acknowledge the use of facilities at the Stanford Synchrotron Radiation Laboratory which is supported by the National Institutes of Health Biomedical Research Technology Program, Division of Research Resources, and by the U.S. Department of Energy, Basic Energy Sciences (BES), and Office of Biological and Environmental Research.

Note Added in Proof. During the review of this manuscript, a paper by Horng et al. describing the UV/vis and X-band EPR of human Sco1 and Sco2 was published. (Horng, Y.; Leary, S. C.; Cobine, P. A.; Young, F. B. J.; George, G. N.; Shoubridge, E. A.; Wing, D. R. *J. Biol. Chem.* **2005**, 34113−34121.) In this work, mutation of D238 to Ala bleached the Cu(II) chromophore but had no effect on Cu(I) binding. Thus, it is probable that an analogous aspartate residue in BSco may be the origin of the oxygenic ligand inferred from the EXAFS and ENDOR.

Supporting Information Available: Extended discussion of parameters obtained by simulations of EPR spectra, analysis of nitrogen quadrupole ESEEM peaks, analysis of β-methylene splittings, analysis of exchangeable proton splittings, SIMPIPM program, experimental and simulated X-band ENDOR spectra of Cu^{II}BSco in H_2O (Figure S1), and experimental and simulated second-derivative X-band EPR spectra of Cu^{II}BSco in D_2O (Figure S2). This material is available free of charge via the Internet at http://pubs.acs.org.

JA0529539

(92) In 26 structures with ZnS_2N_2 coordination listed in the Cambridge database, the average Zn−S distance was 2.280 Å and the average Zn−N distance was 2.072 Å.
(93) Laity, J. H.; Lee, B. M.; Wright, P. E. *Curr. Opin. Struct. Biol.* **2001**, *11*, 39−46.
(94) Zhou, Z. Z.; Peariso, K.; Penner-Hahn, J. E.; Mathews, R. G. *Biochemistry* **1999**, *38*, 15915−15926.
(95) Peariso, K.; Zhou, Z. S.; Smith, A. E.; Matthews, R. G.; Penner-Hahn, J. E. *Biochemistry* **2001**, *40*, 987−993.
(96) Harris, C. M.; Derdowski, A. M.; Poulter, C. D. *Biochemistry* **2002**, *41*, 10554−10562.
(97) In 55 structures with square planar NiS_2N_2 coordination listed in the Cambridge database, the average Ni−S distance was 2.168 Å and the average Ni−N distance was 1.933 Å. In 10 structures with tetrahedral NiS_2N_2 coordination, the average Ni−S distance was 2.246 Å and the average Ni−N distance was 1.983 Å.
(98) Wuerges, J.; Lee, J. W.; Yim, Y. I.; Yim, H. S.; Kang, S. O.; Carugo, K. D. *Proc. Natl. Acad. Sci. U.S.A.* **2004**, *101*, 8569−8574.
(99) Barondeau, D. P.; Kassmann, C. J.; Bruns, C. K.; Tainer, J. A.; Getzoff, E. D. *Biochemistry* **2004**, *43*, 8038−8047.
(100) Colpas, G. J.; Maroney, M. J.; Bagyinka, C.; Kumar, M.; Willis, W. S.; Suib, S. L.; Mascharak, P. K.; Baidya, N. *Inorg. Chem.* **1991**, *30*, 920−928.